RSC Advances

PAPER

View Article Online
View Journal | View Issue



Cite this: *RSC Adv.*, 2020, **10**, 10038

# Reducing interfacial resistance of a $Li_{1.5}Al_{0.5}Ge_{1.5}(PO_4)_3$ solid electrolyte/electrode interface by polymer interlayer protection†

Leidanyang Wang,[a] Da Liu,[b] Tao Huang,[a] Zhen Geng[c] and Aishui Yu *[ab]

Received 28th January 2020
Accepted 3rd March 2020

DOI: 10.1039/d0ra00829j

rsc.li/rsc-advances

High interfacial resistance of an electrode/electrolyte interface is the most challenging barrier for the expanding application of all-solid-state lithium batteries (ASSLBs). To address this challenge, poly(propylene carbonate)-based solid polymer electrolytes (PPC-SPEs) were introduced as interlayers combined with a $Li_{1.5}Al_{0.5}Ge_{1.5}(PO_4)_3$ (LAGP) solid state electrolyte (SSE), which successfully decreased the interfacial resistance of the SSE/electrolyte interface by suppressing the reduction reaction of $Ge^{4+}$ against the Li metal, as well as producing intimate contact between the cathode and electrolyte. This work provides a systematic analysis of the interfacial resistance of the cathode/SSE, Li/SSE and the polymer/LAGP interfaces. As a consequence, the interfacial resistance of the Li/SSE interface decreased about 35%, and the interfacial resistance of the cathode/SSE interface decreased from $3.2 \times 10^4$ to 543 Ω $cm^2$. With a PPC–LAGP–PPC sandwich structure composite electrolyte (PLSSCE), the all-solid-state $LiFePO_4$/Li cell showed a high capacity of 148.1 mA h $g^{-1}$ at 0.1C and a great cycle performance over 90 cycles.



## Introduction

Security is one of the most important issues that needs to be considered for the large-scale application of Li secondary batteries with both higher energy densities and long cycle life.[1] However, safety issues have been increasingly prominent with the significant development of commercial lithium-ion batteries (LIBs) in recent decades, for example, battery explosions and fire caused by thermal runaway behavior, formation and uncontrolled growth of Li-dendrites, which leads to a short circuit and finally death of the LIB. All of these are due to the presence of the organic liquid electrolytes, which are flammable, volatile and toxic. Furthermore, the application of high-voltage cathodes in LIBs is also limited by the intrinsic electrochemical window of the organic liquid electrolyte.[2,3] The all-solid state lithium battery (ASSLB) is recognized as the best candidate for next-generation energy storage with many advantages, such as effective suppression of lithium dendrite growth, higher energy density and excellent security, as well as thermal stability, due to replacing the liquid electrolyte with a solid state electrolyte (SSE).[4] Li-conductive ceramics combine a strong mechanical stiffness, a high $Li^+$ transfer number and acceptable ionic conductivity at room temperature.[5,6] Unfortunately, the huge impedance at the composite cathode/SSE interface[7,8] and the instability of SSE relative to Li metal presented in all solid-state batteries have initiated volume expansion or other contact issues, leading to a serious degradation of battery performance.[9]

NASICON-type solid electrolyte has a relatively high ionic conductivity, and the LAGP SSEs exhibit the highest ionic conductivity on the order of $10^{-3}$ S $cm^{-1}$ at room temperature.[10,11] Due to the absence of transition metals, LAGP was acknowledged to be stable toward the Li metal for a long time.[12] However, an increased impedance of Li/LAGP interface was observed in cycled cells. Besides, the reduction of Ge as a result of a reaction with the Li metal leads to the formation of interphases, which is responsible for the higher interfacial impedance.[13–16] Kang *et al.* found that the chemically formed interphase between the Li metal and LAGP was a mixture of stoichiometrically altered LAGP and Li-related oxides, which showed a reduction of ionic conductivity and a promotion of electronic conductivity. At 200 °C, a thermal runaway behavior emerged as a consequence of the rigorous chemical reaction between the interphase and Li.[17] To address these challenges, polymer electrolyte layers were proposed to protect the ceramic layer from directly contacting the lithium metal and uniform the $Li^+$ flux on the lithium surface, which inhibit lithium dendrite nucleation.[18–25] Moreover, gel electrolyte interlayers were introduced in ceramic-based solid state batteries, which

[a]*Laboratory of Advanced Materials, Institute of New Energy, Fudan University, Shanghai 200438, China. E-mail: asyu@fudan.edu.cn*

[b]*Department of Chemistry, Shanghai Key Laboratory of Molecular Catalysis and Innovative Materials, Collaborative Innovation Center of Chemistry for Energy Materials, Fudan University, Shanghai 200438, China*

[c]*Shanghai Electric Group Co., Ltd. Central Academe, No. 960 Zhongxing Road, Shanghai, 200070, China*

† Electronic supplementary information (ESI) available. See DOI: 10.1039/d0ra00829j

displayed a remarkable wettability toward the Li surface, with high ionic conductivity at room temperature thanks to the composition of the polymer and liquid.[26,27] However, a detailed analysis of the interfacial resistance of the multilayer LAGP-based composite electrolyte has been rarely reported, and the interaction between the ceramic layer and the polymer layer has yet to be understood.

In this work, solid polymer electrolyte (SPE) layers with a thickness of about 70 μm were introduced between LAGP SSE and the electrodes by a drop-casting method. Fig. 1a displays a schematic of the Li-metal batteries design using the polymer–LAGP multilayer SSE and a bare LAGP pellet. The SPE used in this work is a PPC-based composite electrolyte with the addition of lithium bis(trifluoromethanesulphonyl)imide (LiTFSI), which has been reported to possess superior compatibility with Li metal and helps to construct the electrode/SSE interface with smaller impedance.[28–31] Due to the PPC–LAGP–PPC sandwich structure solid composite electrolyte (PLSSCE) design, the interfacial resistances of LAGP pellet against the electrodes decreased significantly. Our results showed that the symmetric cells with a bare LAGP pellet SSE and Li metal will have a sharply increase of interfacial resistance during electrochemical cycling as a result of the reduction reaction between LAGP and lithium metal. On the contrary, when combined with PPC-based interlayers, the cells can cycled with stable stripping and plating profiles with a low overpotential. The hybrid electrolyte design with polymer interlayers is an important surface engineering strategy to decrease the overall interfacial resistance between electrolytes and electrodes while guaranteeing safe and stable Li-metal batteries with great performance.

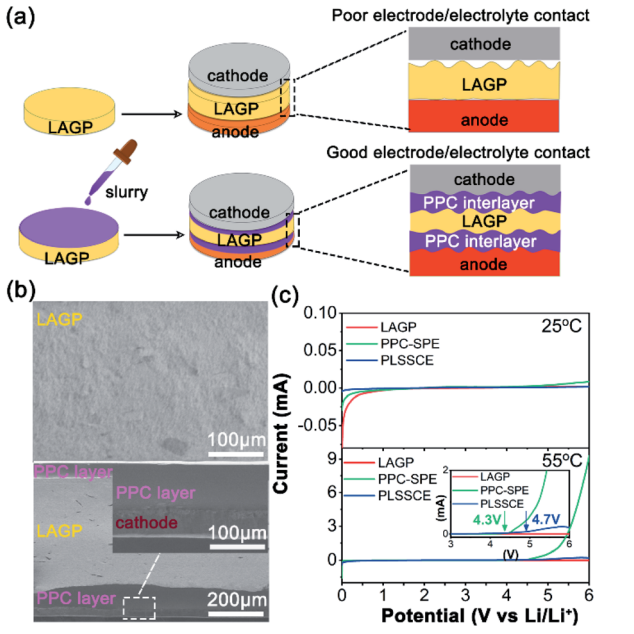


Fig. 1 (a) Schematic of the batteries design with pure LAGP electrolyte and PLSSCE. (b) SEM image of the LAGP surface (top) and the cross-section image of the PLSSCE/$LiFePO_4$ interface (below, with a partially enlarged view of the dotted box) (c) LSV curves obtained for the pure LAGP pellet, PPC-SPE and PLSSCE at 25 °C and 55 °C.

## Results and discussion

The LAGP pellet was prepared by a cold-pressing and sintering process. The cross-sectional SEM image of the cold-pressed LAGP pellet (Fig. S1a†) shows few pores and cracks, while it possessed dense grain structures with an obvious dimension reduction as a result of sintering at 900 °C for 3 h (Fig. S1b and c†). The dense structure enables a homogeneous current distribution and prevents lithium-metal dendrites from penetrating through the electrolyte during cycling with a limited current density.[26] The X-ray diffraction (XRD) pattern of the LAGP pellets (Fig. S1d†) matches well with the $LiGe_2(PO_4)_3$ (PDF# 80-1924) and shows an increase in crystallinity after sintering because of grain boundary fusion. Fig. S1e† shows the impedance diagrams of different LAGP pellets. It can be seen that the LAGP pellet prepared by cold-pressing alone had a huge grain boundary impedance, while it was greatly decreased in the LAGP pellet after a sintering process, thus ensuring a high Li-ion conductivity of $2.61 \times 10^{-4}$ S $cm^{-1}$ at 25 °C. The PLSSCE with double PPC-SPE coatings ($\sigma = 2.9 \times 10^{-5}$ S $cm^{-1}$ at 25 °C) was prepared by a "drop-casting" method, which significantly improved the interfacial contact between the $LiFePO_4$ (LFP) cathode and the rough surface of the ceramic pellet (Fig. 1b). Linear sweep voltammetry (LSV) was verified to examine the electrochemical stability window of the LAGP pellet, PPC-SPE membrane and PLSSCE. As shown in Fig. 1c, the LSV curves of the LAGP and PLSSCE are almost flatness in the voltage range of 0–6.0 V at 25 °C. The PPC-SPE membrane experiences a slight oxidation above 4.9 V. Under the high temperature test conditions (55 °C), the oxidation potential of the SPE membrane decreased to 4.3 V, while the PLSSCE remained electrochemically stable up to 4.7 V. Polymer electrolytes generally have a narrower voltage window, because they are more easily decomposed by Li metal anode under the action of an electric field.[22] Inserting a LAGP ceramic layer could prevent the migration of anion in SPE, which reduces the double-layer electric field at the Li/SPE interface and lowers the electrochemical decomposition of the SPE, facilitating the stability of the PLSSCE. This wide stable voltage range makes the hybrid solid electrolyte suitable for lithium-metal anodes with more cathode materials.

The interfacial impedance analysis between the SSE and electrodes is shown in Fig. 2. The resistances of various interfaces in the Li/electrolyte/Li and cathode/electrolyte/cathode cells are presented in Table 1. Fig. 2a shows the impedance profile of a Li/LAGP/Li symmetric cell. The vast semicircle from high frequencies to 345.5 Hz corresponds to the sum of the bulk and grain boundary impedances of the LAGP pellet ($R_{LAGP}$) and the interfacial resistance of Li/LAGP ($R_{Li/LAGP}$). The $R_{Li/LAGP}$ is about 258.8 Ω $cm^2$ for each side, as calculated with equivalent circuit simulations shown in the ESI, Fig. S2a.† It should be noted that there is a semi-circular tail at low frequency which might be related to the existence of a stagnant Li-ion diffusion layer as a result of the chemically formed interphases between LAGP and Li metal.[17] The impedance profile of the Li/PPC-SPE/Li symmetric cell contains the impedance of SPE ($R_{SPE}$),

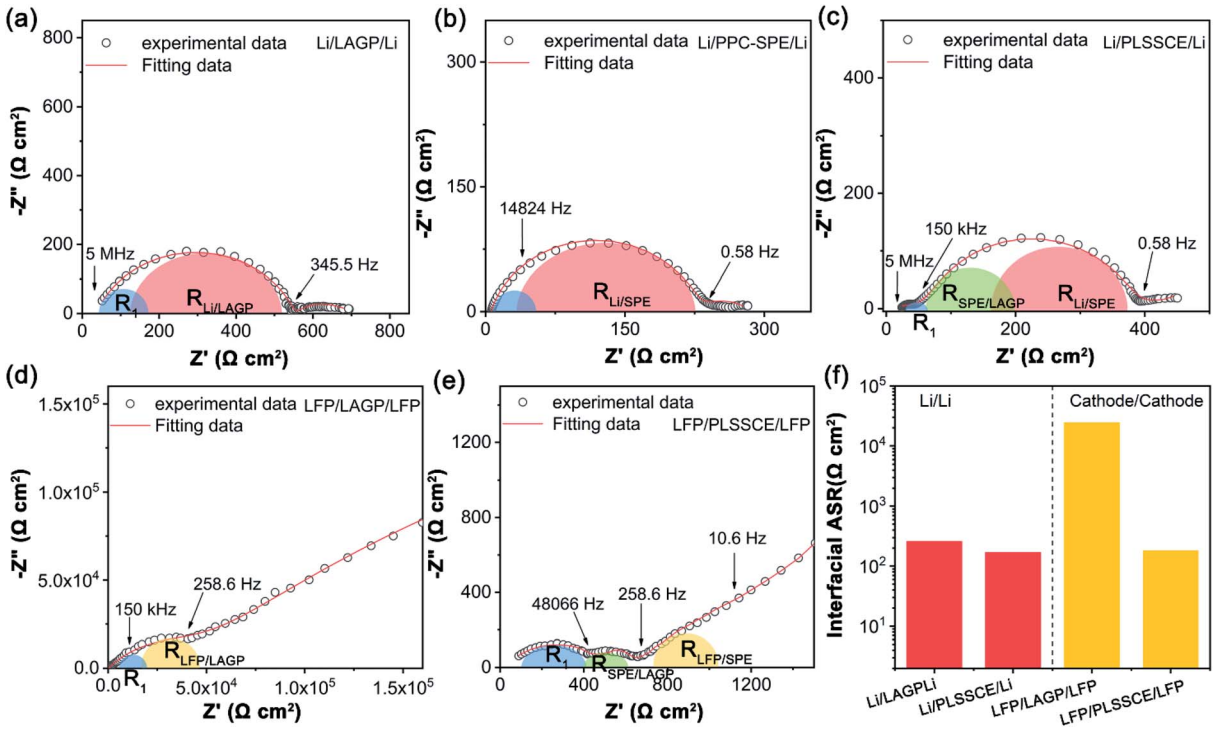


Fig. 2 Impedance analysis of electrolyte/Li and electrolyte/LFP cathode interfaces. (a) EIS of a Li/LAGP/Li symmetric cell. (b) EIS of a Li/PPC-SPE/Li symmetric cell. (c) EIS of a Li/PLSSCE/Li symmetric cell. (d) EIS plot of a LFP/LAGP/LFP symmetric cell. (e) EIS plot of a LFP/PLSSCE/LFP symmetric cell. (f) Comparison of the SSE/electrode interfacial areal specific resistance (ASR) with and without the PPC-SPE interlayers.

interfacial resistance of Li/SPE interfaces ($R_{Li/SPE}$), and diffusion impedance in the low frequency region (Fig. 2b). The $R_{SPE}$ in Li/Li interface was about 34.2 Ω cm$^2$, calculated from the corresponding fitting result in the ESI, Fig. S2b,† which is smaller than that of the SS/PPC-SPE/SS cell (Fig. S1f†). This indicates that the PPC of the interlayer wetted the surface of Li metal by an interfacial reaction, which decreased the bulk resistance and obtained a small interfacial resistance between Li and PPC-SPE ($R_{Li/SPE}$ = 99 Ω cm$^2$). The EIS plot of the Li/PLSSCE/Li symmetric cell (Fig. 2c) contains the internal resistance of the LAGP in the high frequency range, interfacial resistance in the middle frequency range, and the diffusion impedance in the low frequency range. According to the equivalent circuit (Fig. S2c.†), the second semicircle can be divided into $R_{SPE/LAGP}$ and $R_{Li/SPE}$ based on the corresponding frequency intervals. Thanks to the great wettability of the PPC-SPE interlayers, the total interfacial resistance of the Li/PLSSCE/Li cell was 336.9 Ω cm$^2$, which made a 35% decrease in the resistance for Li/LAGP interface.

The interfacial resistances between the cathodes and SSEs were also investigated by a cathode/cathode symmetric cell. In Fig. 2d, the EIS plot shows a huge interfacial resistance for individual LAGP. This may be due to the poor and hard contact between the rough surface of the LAGP pellet and the $LiFePO_4$ (LFP) composite cathode. Besides, the equivalent circuit shows

Table 1 Impedance of the electrode/SSE/electrode symmetric cells

| Symmetric cell | Component | Equivalent circuit parts | Resistance (Ω cm$^2$) |
|---|---|---|---|
| Li/LAGP/Li | LAGP | $R_b$, $R_g$ $CPE_1$ | 114.7 |
| | Li/LAGP interface | $R_{Li/LAGP}$, $CPE_2$ | 258.8 |
| Li/PPC-SPE/Li | SPE | $R_0$, $R_1$, $CPE_1$ | 34.2 |
| | Li/SPE interface | $R_{Li/SPE}$, $CPE_2$ | 99 |
| Li/PLSSCE/Li | LAGP, SPE | $R_0$, $R_1$, $CPE_1$ | 104.6 |
| | SPE/LAGP interface | $R_{SPE/LAGP}$, $CPE_2$ | 75.2 |
| | Li/SPE interface | $R_{Li/SPE}$, $CPE_3$ | 93.4 |
| LFP/LAGP/LFP | LAGP, interphase | $R_1$, $CPE_1$ | 2967 |
| | LFP/LAGP interface | $R_{LFP/LAGP}$, $CPE_2$ | 15 963 |
| LFP/PLSSCE/LFP | LAGP, SPE | $R_0$, $R_1$ $CPE_1$ | 326.5 |
| | SPE/LAGP interface | $R_{SPE/LAGP}$, $CPE_2$ | 111 |
| | LFP/SPE interface | $R_{LFP/SPE}$, $CPE_3$ | 160.5 |

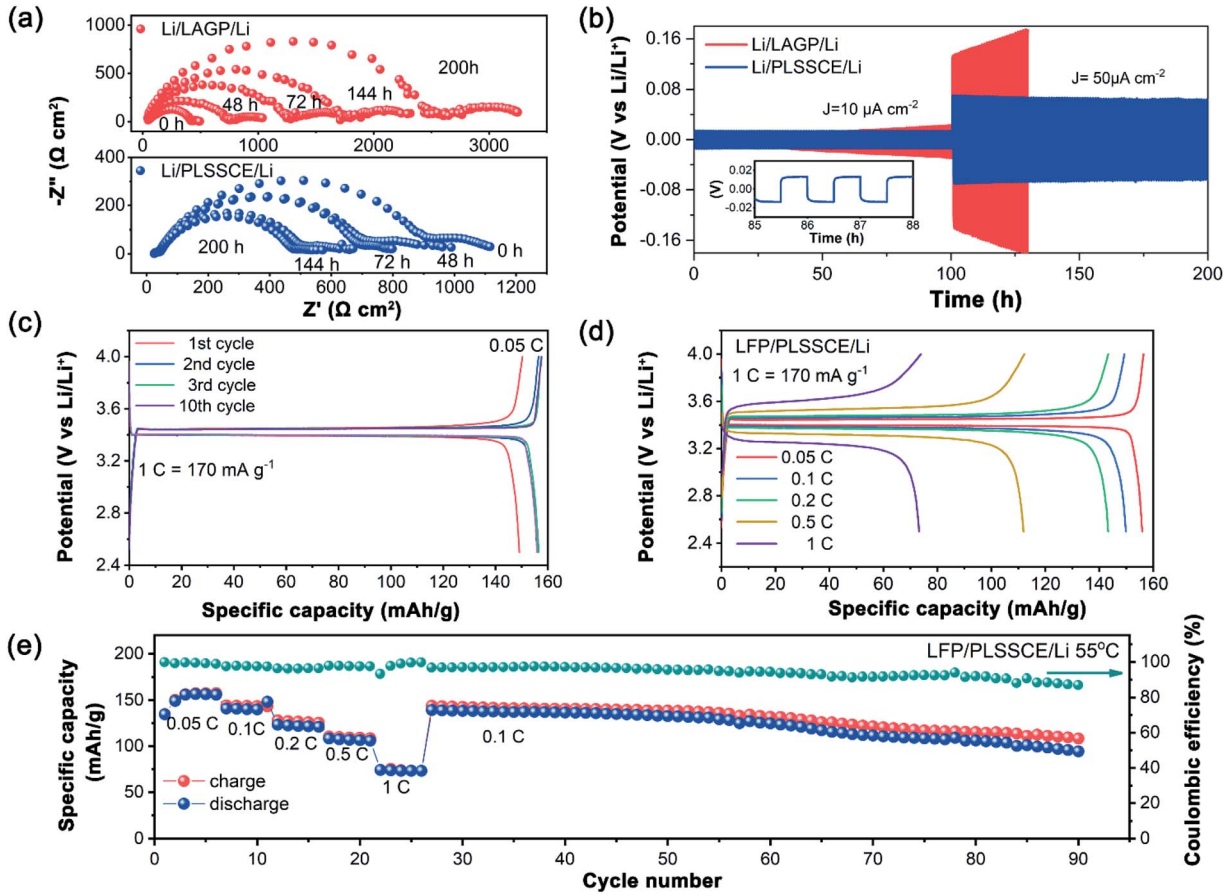


Fig. 3 (a) The Nyquist plots of the bare LAGP (red) and PLSSCE (blue) in Li/Li symmetric cells. (b) The long-term cycling of Li/Li symmetric cells with bare LAGP (red) and PLSSCE (blue) tested at different current densities. (c) Charge–discharge profiles of LFP/PLSSCE/Li cell at 0.05C. (d) Charge–discharge profiles of LFP/PLSSCE/Li cell at different rates. (e) Rate performance of LFP/PLSSCE/Li cell at 55 °C and the cycling performances at 0.1C.

a value of 2967 Ω cm$^2$ ($R_1$) for LAGP resistance, which is much larger than that in the Li/Li symmetric cell. The underlying cause of such high resistance is speculated to be the formation of some interphases as a result of the reactions between the cathode and the solid electrolyte, which occur in various inorganic oxide-based solid electrolytes.[32,33] Unfortunately, the impedance for these interphases could not be distinguished clearly in the fitting circuit. The EIS plot of LFP/PLSSCE/LFP exhibits three sections according to the fitting curve (Fig. 2e). (1) The first semicircle in the high frequency region, which referred to a sum of ionic resistance of LAGP and PPC-SPE layers ($R_1 = 326.6$ Ω cm$^2$). (2) The second semicircle of intermediate frequency region, which referred to the interfacial resistance of SPE/LAGP ($R_{SPE/LAGP} = 111$ Ω cm$^2$). (3) A semicircle impedance at the front of the tail in the low frequency range may belongs to the interfacial resistance between LFP and PPC-SPE ($R_{LFP/SPE} = 160.5$ cm$^2$). Compared with the Li/Li symmetric cell, the PPC-SPE interlayer is more effective at improving the cathode/SSE interface.

Therefore, the LAGP-based sandwich structure hybrid electrolytes with the PPC-SPE interlayers can significantly reduce the interfacial resistance between the LAGP pellet and the electrodes, including both cathodes and Li-metal anodes, as shown in Fig. 2f. The total interfacial impedance between the electrolyte and lithium metal decreased by about 180 Ω cm$^2$, while it was reduced more obviously in the cathode/electrolyte interface from 3.2 × 10$^4$ to 543 Ω cm$^2$ after applying the PPC-SPE interlayers, which is acceptable for ASSLBs.

Stability of the Li/SSE interface was analyzed by repeated impedance analysis over 200 h. During the initial stage, Li/LAGP/Li had a low interfacial resistance. This value grew rapidly and climbed to over 2000 Ω cm$^2$ after 150 h (Fig. 3a). In addition, a semicircle tail appeared in the low frequency region with size expansion. This is mainly due to the formation of interphases caused by chemical reactions between the Li and LAGP, leading to an interruption of Li-ion diffusion. This phenomenon also existed in the interfacial impedance test above. On the contrary, the PLSSCE with PPC coated layers exhibited a reduction of the interfacial resistance during the early stages and became steady with slight change at the end of the experiment (Fig. 3a). The impedance reduced because the PPC electrolyte could diffuse into the bulk LAGP pellet and minimize the interfacial impedance between domains, which was caused by a "wetting reaction" as a result of the Li/PPC contact. The Li/PLSSCE interface showed a lower resistance and higher stability compared with the bare

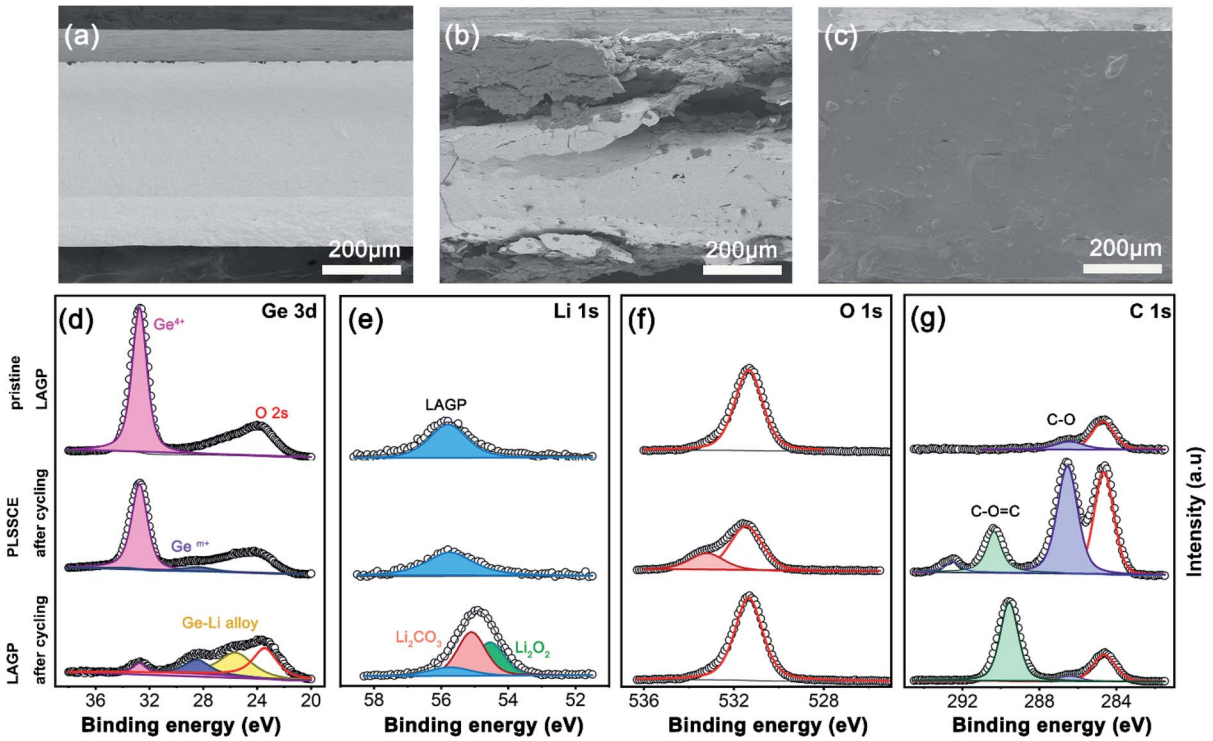


Fig. 4 (a) Cross-sectional SEM image of pure LAGP pellet before electrochemical cycling. Cross-sectional SEM image of pure LAGP (b) and PLSSCE electrolyte (c) after electrochemical cycling. XPS analysis of (d) Ge 3d, (e) Li 1s, (f) O 1s, and (g) C 1s peaks on the surfaces of LAGP (pristine pellet), PLSSCE (obtained from the Li/PLSSCE/Li cell after 50 cycles at 0.05 mA $cm^{-2}$), LAGP (obtained from the Li/LAGP/Li cell after 50 cycles at 0.05 mA $cm^{-2}$).

LAGP, besides, the existence of PPC-SPE separated the Li and LAGP, effectively eliminating the formation of interphases with low ionic conductivity. To further investigated the electrochemical performance of the PLSSCE toward Li metal, galvanostatic cycling tests of Li/Li cells were performed and are shown in Fig. 3b. The overpotential of bare LAGP cell increased with different current densities and reached to 169 mV within 25 h at 50 μA $cm^{-2}$, while the cell with PLSSCE pellet showed a stable and smaller overpotential of 13 mV at 10 μA $cm^{-2}$, the value changed to 55 mV at 50 μA $cm^{-2}$ and was constant after 200 h (Fig. 3b), demonstrating that the PPC-SPE interlayers can yield stable Li plating and stripping.

The electrochemical performances of the LFP/Li solid state batteries (SSBs) were tested through galvanostatic charge/discharge at 55 °C. The LFP/PLSSCE/Li cell exhibited an approximate discharge specific capacity of 156.5 mA h $g^{-1}$ with liquid based LFP/Li cells at 0.05C with a typical charge–discharge curve (Fig. 3c). The LFP/LAGP/Li all-solid-state cell barely worked without the PPC-SPE interlayer, as shown in Fig. S3,† which owing to the huge internal resistance. There was a slight increase in capacity and a polarization voltage reduction of the first few cycles due to the activation of LFP and improved contact between the electrolyte/electrode interfaces, then the capacities and the voltage platform remained stable with insignificant changes. The excellent cycling performance can be explained by the stability of the PPC-SPE protected SSE, as well as the satisfactory interface compatibility of the electrode and electrolyte. The rate capabilities of the cells within a voltage range 2.5–4.0 V at 55 °C are shown in Fig. 3d. As the current density increased, the cell offered high discharge capacities of about 148.1, 143.3 and 111.9 mA h $g^{-1}$ at rates of 0.1, 0.2 and 0.5C, respectively. At a higher current of 1.0C, the capacity of the LFP/PLSSCE/Li cell faded to 78.9 mA h $g^{-1}$ with a higher voltage plateau. The capacity degradation is due to the limited ionic conductivity and increased cell polarization. After the end of cycling at 1.0C, the discharge specific capacities were boosted to 139.2 mA h $g^{-1}$ upon returning the rate back to 0.1C, reaching 94.5% of the discharge capacity of the last cycle at 0.1C (Fig. 3e). At the end of the continued 90 cycles, the cell still obtained a capacity of 98.9 mA h $g^{-1}$, verifying that the PLSSCE can function effectively as a SSE in a lithium battery.

We disassembled the cells after electrochemical cycling and observed the morphology of the electrolytes. As shown in Fig. 4a–c, the pristine LAGP pellet showed flat and clean edges with a high compactness. After a long-term impressed current, the bare LAGP pellet showed serious pulverization intuitively and turned black in colour. There were many large cracks in the main body of the LAGP pellet and a thick layer grew on the surface of each side (Fig. 4b). This serious structural destruction may be the main reason for the increased impedance. However, the structural pulverization was not found in the PLSSCE based Li/Li symmetrical battery after cycling. The electrolyte remained integrated and had a smooth surface with a polymer filling (Fig. 4c).

 

X-ray photoelectron spectroscopy (XPS) was measured to comprehensively understand the surface chemistry of the interfaces of the bare LAGP pellet and PLSSCE. The XPS spectra of different SSEs were taken from the electrolyte side in Li/SSE interface with same areas and the results are shown in Fig. 4d–g. The Ge 3d, Li 1s, O 1s and C 1s spectra of LAGP pellet with and without PPC-SPE interlayers were obviously different after electrochemical cycling. The pristine LAGP showed a sharp peak at 32.8 eV, which corresponds to $Ge^{4+}$ and the O 2s peak at 23.5 eV.[14,15] After cycling, the $Ge^{4+}$ peak was observed with a low intensity for the Li/LAGP/Li cell and two new peaks with lower binding energy, representing a lower chemical state of Ge ($Ge^{m+}$, 28.4 eV) and Li–Ge alloy (25.6 eV).[14,34] These results give the evidence for the reduction of $Ge^{4+}$ in LAGP by Li metal and the formation of interphase. The Li 1s peak of Li/LAGP interface shifted to a lower binding energy with an increased intensity as shown in Fig. 4e. The formation of $Li_2O_2$ and $Li_2CO_3$ may be ascribed to a combination of escaped O and diffused Li-ions produced by $Ge^{4+}$ reduction according to the deconvolution results.[17,35] Stoichiometric changed LAGP were observed on the surface of the LAGP pellet with dominating electronic conductivity,[17] which caused the mechanical deterioration of the LAGP pellet (as shown in Fig. 4b) and lead to a gradual increase of the interfacial resistance and cell failure. On the contrary, the Ge 3d line changes slightly in Li/PLSSCE/Li cell after cycling with an inconspicuous, weak peak of $Ge^{m+}$ (28.5 eV), which owing to the reduction of some exposed LAGP at the interface. Moreover, the Li 1s lines were almost the same before and after cycling (55.8 eV), confirming that the LAGP was effectively protected from reduction by the PPC-SPE interlayers by preventing direct contact of LAGP and Li. For O 1s (Fig. 4f) and C 1s (Fig. 4g) spectra, no significant changes could be observed in the O 1s line of Li/LAGP, while a new peak for C 1s at 289.6 eV represented the C=O groups of carbonates,[36] which are regarded as the products of interfacial reactions. Furthermore, the Li/PLSSCE interface only showed peaks at 533.2 eV (C–O, O 1s), 286.5 eV (C–O, C 1s), and 290.3 eV (O–C=O, C 1s) corresponding to the PPC-SPE and its derivatives.[31]

These results imply that the LAGP pellet with PPC-SPE passivation is conductive to inhibiting the growth of interphases caused by the reduction of Ge. Furthermore, the superior cycling stability is attributed to a stable Li/electrolyte interface and effective suppression of Li dendrites.

## Conclusions

We successfully addressed the high interfacial resistance by coupling an LAGP solid electrolyte with the cathode and Li metal by a sandwich structure design for hybrid SSE with PPC-SPE interlayers. Combination with a polymer electrolyte can effectively protect the Li metal and help prolong the cycling lifetime of Li-metal batteries. PPC-SPE is flexible and possesses high ionic conductivity. The excellent wettability of PPC toward electrodes reduced the interfacial resistance of Li/SSE from 517.6 to 337.2 $\Omega\ cm^2$, with an especially significant decrease of the interfacial resistance for LAGP from $3.2 \times 10^4$ to 543 $\Omega\ cm^2$ against the $LiFePO_4$ cathode, which allows ASSLBs to be operated normally with a high capacity of 148.1 mA h $g^{-1}$ for $LiFePO_4$ at 0.1C and a stable cycling performance over 90 cycles at 55 °C. The superior cyclic performance of the LiFePO4/PLSSCE/Li cell is mainly attributed to the effective inhibition of $Ge^{4+}$ reduction as well as derivative side reactions at the Li/LAGP interface, due to the introduction of PPC-SPE interlayers, which not only protected the LAGP pellets from side reactions with lithium metal anodes but also reduced the huge interfacial resistance of solid–solid interfaces during cycling in LIBs.

## Experimental

### Preparation of PLSSCE

The $Li_{1.5}Al_{0.5}Ge_{1.5}P_3O_{12}$ (LAGP) powders (Hefei Kejing Materials Technology CO., LTD) were placed in a stainless-steel mold and pressed at ~60 MPa for 1 min to form a pellet. Then the LAGP pellets were sintered in a tube furnace at 900 °C for 3 h in air. The as-prepared pellets were obtained with a diameter of 16.5 mm and thicknesses between 400 and 450 μm. The cold-pressed LAGP pellets without high temperature sintering were also prepared as control.

PPC-based coating layer was made by dissolving 1 g PPC (PPC, $M_n \sim 50\,000$, Sigma-Aldrich) and 0.2 g LiTFSI (Sigma-Aldrich) into 3 mL acetone solvent under mechanical stirring for 1 h to get a homogeneous solution. The solution was dropped on each side of LAGP pellet and dried first at 25 °C for 8 h and then at 60 °C in a vacuum oven for 12 h to form a SPE membrane. The PLSSCEs were obtained and the thickness of the SPE membrane was controlled at about 70 μm. Single PPC-SPE used cellulose separator as a supporting membrane were prepared *via* a similar method.

### Material characterization

The morphology of LAGP pellet and as-prepared PLSSCE were examined by a field emission scanning electron microscope (FE-SEM, Hitachi-S4800). Phase analysis was performed by XRD on a D8 Advanced diffractometer (Bruker, Germany) using Cu-Kα radiation operated at 40 kV and 40 mA in the $2\theta$ range from 10° to 80°. The X-ray photoelectron spectroscopy (XPS) was employed to detect the surface composition using a RBD upgraded PHI-5000C ESCA system (PerkinElmer Co., USA) with Al Kα radiation ($h\nu = 1486.6$ eV).

### Battery fabrication and electrochemical test

To prepare the cathodes, PPC and LiTFSI were dissolved in a certain amount of *N*-methyl-2-pyrrolidone (NMP) to get a viscous solution. $LiFePO_4$, LAGP and SP were mixed in agate mortar and then added into the solution and vibrated for 1 h. The obtained slurry with a mass ratio $LiFePO_4$ : LAGP : PPC : SP = 7 : 1 : 1.5 : 0.5 was casted onto a carbon coated Al foil and vacuum dried at 80 °C for 12 h. The active material loading of every cathode electrode ($\Phi = 12$ mm) was about 2.49 mg $cm^{-2}$. The 2032 coin cells were fabricated in an argon-filled glove box with lithium sheets (China Energy Lithium Co., Ltd. $\Phi = 15$

mm, $\delta = 0.6$ mm) as the anode, and preheated at 80 °C for 12 h before testing.

The ionic conductivity of the as-prepared LAGP pellet was tested by electrochemical impedance spectroscopy (EIS) measurement assembled with stainless steel (SS) electrodes in the frequency range of 1 Hz to 5 MHz with the alternative current amplitude of 5 mV and calculated by eqn (1):

$$\sigma = L/RS \quad (1)$$

where $R$, $L$ and $S$ represent the resistance value, the thickness of the sample and the test area, respectively.

Linear sweep voltammetry (LSV) was conducted on the Li/SSE/SS coin cells with stainless-steel as a working electrode and lithium metal as a counter electrode tested from 0 to 6.0 V *vs.* $Li/Li^+$ at a speed of 1 mV $s^{-1}$ (the unit of potential mentioned in this paper is V *vs.* $Li/Li^+$). LSV and EIS were measured on the Bilogic-VSP300 electrochemical workstation. Lithium plating/stripping test was operated on symmetric Li/Li cells with the electrolytes at different current densities (10 μA $cm^{-2}$, 50 μA $cm^{-2}$) with a period of 30 min to evaluate the stability between the SSEs and the Li anodes. The $LiFePO_4$/PLSSCE/Li (LFP/PLSSCE/Li) all solid state cells were performed on a LAND testing system (CT2001A, Wuhan, China) at 55 °C between 2.5–4.0 V of varied currents (1C = 170 mA $g^{-1}$). As a comparison, $LiFePO_4$/LAGP/Li cells without PPC-SPE interlayers were assembled and tested at 55 °C.

The interfacial impedance was measured for both the Li/SSE interface and the $LiFePO_4$ cathode/SSE interface. Symmetric cells (Li/electrolyte/Li, $LiFePO_4$/electrolyte/$LiFePO_4$) were made and preheated at 80 °C for 12 h before the EIS test with a voltage amplitude of 5 mV and a frequency range from 0.01 Hz to 5 MHz.

## Conflicts of interest

There are no conflicts of interest to declare.

## Acknowledgements

This work was supported by the Science and Technology Commission of Shanghai Municipality (19DZ2270100) and Shanghai Electric Group Co., Ltd. Central Academe, China.

## References

1 A. Perea, M. Dontigny and K. Zaghib, *J. Power Sources*, 2017, **359**, 182–185.
2 L. Fan, S. Wei, S. Li, Q. Li and Y. Lu, *Adv. Energy Mater.*, 2018, **8**, 1702657.
3 A. Varzi, R. Raccichini, S. Passerini and B. Scrosati, *J. Mater. Chem. A*, 2016, **4**, 17251–17259.
4 R. Chen, W. Qu, X. Guo, L. Li and F. Wu, *Mater. Horiz.*, 2016, **3**, 487–516.
5 J. C. Bachman, S. Muy, A. Grimaud, H. H. Chang, N. Pour, S. F. Lux, O. Paschos, F. Maglia, S. Lupart, P. Lamp, L. Giordano and Y. Shao-Horn, *Chem. Rev.*, 2016, **116**, 140–162.
6 J. W. Fergus, *J. Power Sources*, 2010, **195**, 4554–4569.
7 L. Xu, S. Tang, Y. Cheng, K. Wang, J. Liang, C. Liu, Y.-C. Cao, F. Wei and L. Mai, *Joule*, 2018, **2**, 1991–2015.
8 F. Han, J. Yue, C. Chen, N. Zhao, X. Fan, Z. Ma, T. Gao, F. Wang, X. Guo and C. Wang, *Joule*, 2018, **2**, 497–508.
9 Q. Cheng, A. Li, N. Li, S. Li, A. Zangiabadi, T.-D. Li, W. Huang, A. C. Li, T. Jin, Q. Song, W. Xu, N. Ni, H. Zhai, M. Dontigny, K. Zaghib, X. Chuan, D. Su, K. Yan and Y. Yang, *Joule*, 2019, **3**, 1510–1522.
10 M. J. Hou, F. Liang, K. Chen, Y. N. Dai and D. Xue, *Nanotechnology*, 2020, **31**, 132003.
11 C. R. Mariappan, C. Yada, F. Rosciano and B. Roling, *J. Power Sources*, 2011, **196**, 6456–6464.
12 J. K. Feng, L. Lu and M. O. Lai, *J. Alloys Compd.*, 2010, **501**, 255–258.
13 P. Hartmann, T. Leichtweiss, M. R. Busche, M. Schneider, M. Reich, J. Sann, P. Adelhelm and J. Janek, *J. Phys. Chem. C*, 2013, **117**, 21064–21074.
14 L. He, Q. Sun, C. Chen, J. A. S. Oh, J. Sun, M. Li, W. Tu, H. Zhou, K. Zeng and L. Lu, *ACS Appl. Mater. Interfaces*, 2019, **11**, 20895–20904.
15 S. Kim, S. Won Hwang, S.-H. Choi, R. G. Elliman, Y.-M. Kim and Y.-J. Kim, *J. Appl. Phys.*, 2009, **105**, 106112.
16 Y. Meesala, C.-Y. Chen, A. Jena, Y.-K. Liao, S.-F. Hu, H. Chang and R.-S. Liu, *J. Phys. Chem. C*, 2018, **122**, 14383–14389.
17 H. Chung and B. Kang, *Chem. Mater.*, 2017, **29**, 8611–8619.
18 S.-J. Tan, X.-X. Zeng, Q. Ma, X.-W. Wu and Y.-G. Guo, *Electrochem. Energy Rev.*, 2018, **1**, 113–138.
19 D. Li, L. Chen, T. S. Wang and L. Z. Fan, *ACS Appl. Mater. Interfaces*, 2018, **10**, 7069–7078.
20 Z. Zhang, Y. Zhao, S. Chen, D. Xie, X. Yao, P. Cui and X. Xu, *J. Mater. Chem. A*, 2017, **5**, 16984–16993.
21 D. Bosubabu, J. Sivaraj, R. Sampathkumar and K. Ramesha, *ACS Appl. Energy Mater.*, 2019, **2**, 4118–4125.
22 W. D. Zhou, S. F. Wang, Y. T. Li, S. Xin, A. Manthiram and J. B. Goodenough, *J. Am. Chem. Soc.*, 2016, **138**, 9385–9388.
23 W. Q. Zhang, J. H. Nie, F. Li, Z. L. Wang and C. Q. Sun, *Nano Energy*, 2018, **45**, 413–419.
24 J. Peng, L.-N. Wu, J.-X. Lin, C.-G. Shi, J.-J. Fan, L.-B. Chen, P. Dai, L. Huang, J.-T. Li and S.-G. Sun, *J. Mater. Chem. A*, 2019, **7**, 19565–19572.
25 G. Hou, X. Ma, Q. Sun, Q. Ai, X. Xu, L. Chen, D. Li, J. Chen, H. Zhong, Y. Li, Z. Xu, P. Si, J. Feng, L. Zhang, F. Ding and L. Ci, *ACS Appl. Mater. Interfaces*, 2018, **10**, 18610–18618.
26 B. Y. Liu, Y. H. Gong, K. Fu, X. G. Han, Y. G. Yao, G. Pastel, C. P. Yang, H. Xie, E. D. Wachsman and L. B. Hu, *ACS Appl. Mater. Interfaces*, 2017, **9**, 18809–18815.
27 Q. Guo, Y. Han, H. Wang, S. Xiong, W. Sun, C. Zheng and K. Xie, *J. Phys. Chem. C*, 2018, **122**, 10334–10342.
28 J. J. Zhang, X. Zang, H. J. Wen, T. T. Dong, J. C. Chai, Y. Li, B. B. Chen, J. W. Zhao, S. M. Dong, J. Ma, L. P. Yue, Z. H. Liu, X. X. Guo, G. L. Cui and L. Q. Chen, *J. Mater. Chem. A*, 2017, **5**, 4940–4948.

 

29 J. Zhang, J. Zhao, L. Yue, Q. Wang, J. Chai, Z. Liu, X. Zhou, H. Li, Y. Guo, G. Cui and L. Chen, *Adv. Energy Mater.*, 2015, **5**, 1501082.
30 C. Wang, H. Zhang, J. Li, J. Chai, S. Dong and G. Cui, *J. Power Sources*, 2018, **397**, 157–161.
31 L. D. Y. Wang, S. M. Hu, J. M. Su, T. Huang and A. S. Yu, *ACS Appl. Mater. Interfaces*, 2019, **11**, 42715–42721.
32 J. P. Robinson, P. D. Kichambare, J. L. Deiner, R. Miller, M. A. Rottmayer and G. M. Koenig, *J. Am. Ceram. Soc.*, 2018, **101**, 1087–1094.
33 T. Kato, T. Hamanaka, K. Yamamoto, T. Hirayama, F. Sagane, M. Motoyama and Y. Iriyama, *J. Power Sources*, 2014, **260**, 292–298.
34 Y. Liu, C. Li, B. Li, H. Song, Z. Cheng, M. Chen, P. He and H. Zhou, *Adv. Energy Mater.*, 2018, **8**, 1702374.
35 Q. Yu, D. Han, Q. Lu, Y. B. He, S. Li, Q. Liu, C. Han, F. Kang and B. Li, *ACS Appl. Mater. Interfaces*, 2019, **11**, 9911–9918.
36 J.-Y. Wu, S.-G. Ling, Q. Yang, H. Li, X.-X. Xu and L.-Q. Chen, *Chin. Phys. B*, 2016, **25**, 078204.